BILINGUAL PUBLISHING GROUP

Journal of Environmental & Earth Sciences

https://journals.bilpubgroup.com/index.php/jees

ARTICLE

Research on Accurate Fire Point Positioning Technology in the Forest Region of Northeast China Based on Aerial Photography

Yingyu An [1], *Yang Ju* [1], *Shuxin Han* [2*], *Shuang Wu* [2], *Xiaolei Su* [2]

[1] *Artificial Precipitation Office of Heilongjiang Provincial People's Government, Harbin 150030, China*

[2] *Heilongjiang Eco-Meteorology Center, Harbin 150030, China*

ABSTRACT

Forest fires are one of the most destructive natural disasters to global ecosystems, and accurate and rapid fire point positioning is crucial for forest fire management. In this study, we propose an accurate fire point positioning technology based on aerial photography. This method uses a high-accuracy Global Positioning System and an inertial measurement unit to record the flight attitude and location information of an aircraft, and then it employs precise correction to convert camera coordinates to the aircraft body coordinate system. Finally, this method utilizes a weighted error correction algorithm to fuse the information from multiple images, thereby achieving accurate fire point positioning. To verify the effectiveness of the fire point positioning method proposed in this research, two fire points in the Greater Khingan Region of Heilongjiang Province are selected for verification. A Yun-12 aircraft equipped with a high-accuracy positioning and image-recording sensor was used for fire point observations. The longitude, latitude, flight altitude, roll angle, pitching angle and yaw angle of the aircraft are recorded in real time during image capture. Images of fire points at different angles were captured from multiple flight routes, and they are used to verify the performance and accuracy of the fire point positioning model. The comparison of the latitude and longitude information between estimated and observed fire points indicates that the errors of fire point positioning are reduced to less than 160 m in the model. This represents a 5–6 fold improvement in positioning accuracy over current meteorological-satellite-based kilometer-scale fire point positioning methods, highlighting the notable

*CORRESPONDING AUTHOR:

Shuxin Han, Heilongjiang Eco-Meteorology Center, Harbin 150030, China; Email: brian_hanks@163.com

ARTICLE INFO

Received: 1 April 2026 | Revised: 23 April 2026 | Accepted: 27 April 2026 | Published Online: 22 May 2026

DOI: https://doi.org/10.30564/jees.v8i5.13175

CITATION

An, Y., Ju, Y., Han, S., et al., 2026. Research on Accurate Fire Point Positioning Technology in the Forest Region of Northeast China Based on Aerial Photography. Journal of Environmental & Earth Sciences. 8(5): 200–213. DOI: https://doi.org/10.30564/jees.v8i5.13175

potential of this technique for precise forest fire positioning.

Keywords: Fire Point Positioning; Coordinate Conversion; Error Correction; Measurement

1. Introduction

Forest fires are among the most severe natural disasters affecting global ecosystems, leading to the destruction of biodiversity, soil degradation, reduced water source, and intensified carbon emission, thereby contributing to climate change [1,2]. Early identification and precise monitoring of fire points are crucial for improving the efficiency of forest fire emergency response [3,4].

Satellite remote sensing technology, with the observational advantages of multiple sensors across the visible and infrared spectra, can achieve near-real-time fire detection [5–8]. However, this technology is susceptible to cloud cover and smoke/dust, which have been proven to greatly affect the accuracy of fire point monitoring [9,10]. In addition, the relatively low spatial resolution of current meteorological satellites easily leads to the mixed pixel effect [11–13], which can further affect the accuracy of fire point monitoring [14,15]. Aerial photography, which uses advanced sensors and high-resolution cameras, can effectively capture surface variations and provide real-time and high-resolution fire images, even over complex terrain [16–18] and under low visibility conditions caused by smoke [19–21]. Additionally, unlike satellite-based observations constrained by orbits, aerial photography offers greater flexibility, allowing adaptive monitoring strategies and flight path adjustments in real time according to fire situations to achieve dynamic monitoring. Multi-angle image acquisition enhances the ability to accurately assess fire location, burned area, fire line length and spread direction [22,23]. Aerial photography provides crucial support for the precise extraction of fire points and the enhancement of fire monitoring capabilities.

In recent years, aerial photogrammetry technology has made remarkable progress in forest fire research. Structure from Motion (SfM) by unmanned aerial vehicles and direct georeferencing (DG) are commonly used methods in the positioning detection of forest fires by aerial measurement. The SfM method reconstructs the three-dimensional structure of fire scenes and camera trajectories by analyzing multi-angle fire images [24–26], enabling accurate fire source positioning without relying on the Global Positioning System (GPS) and inertial measurement unit (IMU) data [27,28]. Using the SfM method to reconstruct the three-dimensional model of a fire scene can effectively determine the fire scope and the influenced area [29]. However, the accuracy of the SfM is highly dependent on the quality of input images, i.e., factors such as shooting conditions and lighting variations—which affect image quality—may reduce model performance and thus affect the accuracy of fire source positioning [30]. In comparison, the DG method directly geolocates fire sources in acquired images [31,32] using the position and attitude data of aircraft obtained by the airborne GPS and IMU during aerial photography. This method can provide near-real-time and high-accuracy geographical information, which is crucial for rapid response to forest fire disasters, fire impact assessment and firefighting strategy formulation. The adoption of the DG method can improve the responsiveness of the mobile mapping system for real-time monitoring of forest fires, and offers remarkable advantages in the accuracy and timeliness of fire monitoring [33]. Moreover, DG technology plays an essential role in the application of forest fire models, especially in the aspects of rapid positioning and fire behavior prediction [34]. Nevertheless, DG technology typically relies on fixed-wing aircraft and unmanned aerial vehicles, which are easily affected by complex terrain and meteorological conditions. As a result, there is some drift in the positioning accuracy [35].

Aerial fire point positioning has greatly simplified field operations [36], but real-time fire information extraction and precise fire localization remain significant practical challenges [37]. Here, we introduce a novel DG positioning method that leverages the dynamic monitoring capabilities of airborne platforms. Our approach integrates a ground target coordinate solution model, a precise camera-to-airframe coordinate system transformation, and an unknown point coordinate solving algorithm. Using fixed ground features as Ground Control Points (GCPs), we estimate the camera's effective position and mitigate the impact of camera attitude angle errors through accurate coordinate transformation. We also designed a multi-image weighted error correction algorithm to further refine fire point localization accuracy.

We validated the proposed method using two test fire points in the Greater Khingan region of Heilongjiang Province. Experimental results show that compared with satellite remote sensing-based forest fire monitoring methods[38], our approach delivers clear improvements in both timeliness and positioning accuracy, with errors consistently below 160 meters. This work offers a practical approach for rapid and accurate forest fire monitoring, enabling faster and more targeted fire suppression efforts.

2. Materials and Methods

2.1. Study Area

The study area in this research is the Greater Khingan Region, Heilongjiang Province, Northeast China (**Figure 1**). As an important component of the Khingan Mountains, the Greater Khingan Region is located in the northeast of the Inner Mongolia Autonomous Region and the northwest of Heilongjiang Province (43.0° N–53.5° N, 117.3° E–126.0° E), with an east-west distance of 1,400 km, a south-north distance of 200–400 km, elevations of 1,100–1,400 m, and a total area of about 327,200 km^2. Among them, the area of the Greater Khingan Region within Heilongjiang Province is about 84,800 km^2. The Greater Khingan forest acts as a natural green barrier of the Songnen Plain and Hulunbuir Grassland, and is one of the important forestry bases in China.

2.2. Study Methods

In this study, the fire point positioning model is established by integrating a ground-target coordinate measurement model, a transformation from the camera coordinate system to the aircraft-body coordinate system, and a solution for the coordinates of unknown target points. In order to improve positioning accuracy, a multi-image-based weighted error correction algorithm is proposed to achieve the precise geolocation estimation of target fire points.

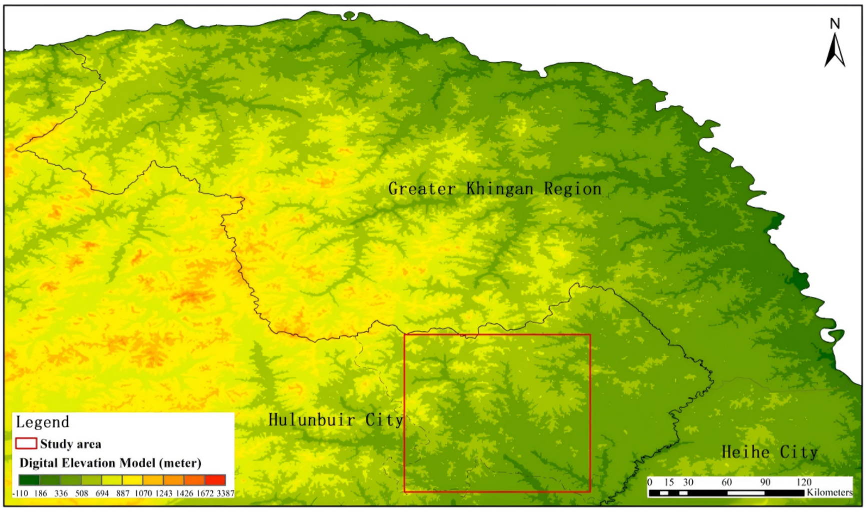

Figure 1. Study area.

2.2.1. Establishment of the Ground-Target Coordinate Measurement Model

The ground-target coordinate measurement model serves as the core component for accurate fire positioning. Based on the positioning information from the GPS and the attitude information from the IMU onboard aircraft during image acquisition, six exterior orientation parameters are determined, i.e., three-dimensional location coordinates of aircraft (X, Y, Z) and its attitude angles (yaw, pitch and roll), which are used in the collinearity equations for geolocation.

Based on the above parameters (**Figure 2**), the spatial relationship among camera coordinates, image pixel points and corresponding ground points can be expressed using the collinearity equations:

$$x - x_0 = -f \frac{a_1 (X_A - X_S) + b_1 (Y_A - Y_S) + c_1 (Z_A - Z_S)}{a_3 (X_A - X_S) + b_3 (Y_A - Y_S) + c_3 (Z_A - Z_S)} \quad (1)$$

$$y - y_0 = -f \frac{a_2 (X_A - X_S) + b_2 (Y_A - Y_S) + c_2 (Z_A - Z_S)}{a_3 (X_A - X_S) + b_3 (Y_A - Y_S) + c_3 (Z_A - Z_S)} \quad (2)$$

Where x and y indicate the coordinates of image pixel points; x_0 and y_0 represent the abscissa and ordinate of the principal point on the phase plane, respectively; f denotes camera focal length and X_S, Y_S and Z_S represent the spatial coordinates of aircraft positions provided by the airborne GPS; X_A, Y_A, and Z_A are the spatial coordinates of corresponding ground points; a_i, b_i and c_i (i = 1, 2 and 3) are the elements of the rotation matrix used to convert ground coordinates to the camera coordinate system.

Among interior orientation parameters, the accuracy of x_0 and y_0 can affect the photogrammetric accuracy, and thus, accurate camera calibration is essential. In this study, the checkerboard calibration method provided by the Open Computer Vision Library is applied for camera calibration[39]. The calibration for interior and exterior orientation parameters is accomplished by open-source library functions. Through calibration, the calibrated interior orientation parameters are $[x_0, y_0, f]$ = [316.2778, 232.4590, 45].

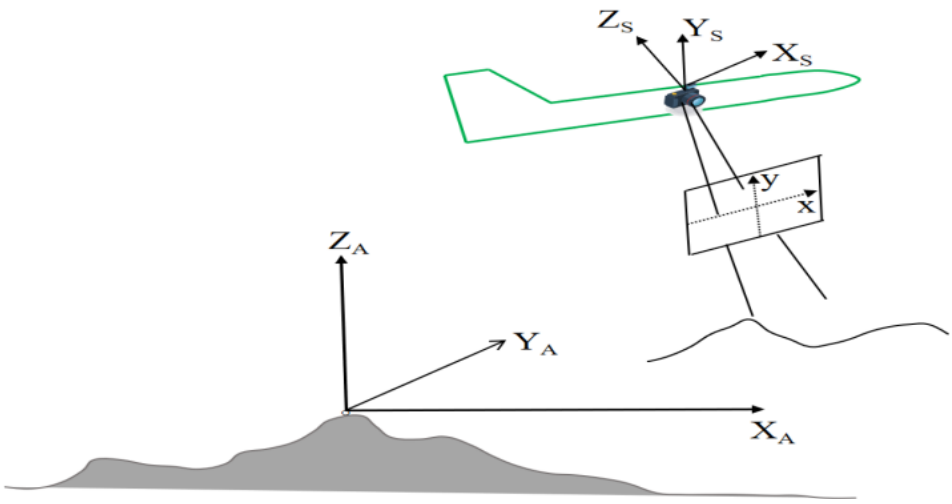

Figure 2. Schematic diagram of fire point positioning by aircraft.

2.2.2. Transformation from the Camera Coordinate System to the Aircraft-Body Coordinate System

During flight, the GPS module onboard the aircraft continuously records its real-time longitude. Combined with the attitude sensor data from the airborne IMU, the attitude information of the aircraft corresponding to the geographic coordinate system can be obtained (**Figure 3**).

In practice, there are measurement errors in the rotation angle of the camera relative to the aircraft body. Therefore, in this study, the optimal transformation matrix is estimated by using the least square method based on the GCPs with known coordinates. Based on this, we can calculate the angle and attitude of the camera relative to the aircraft body.

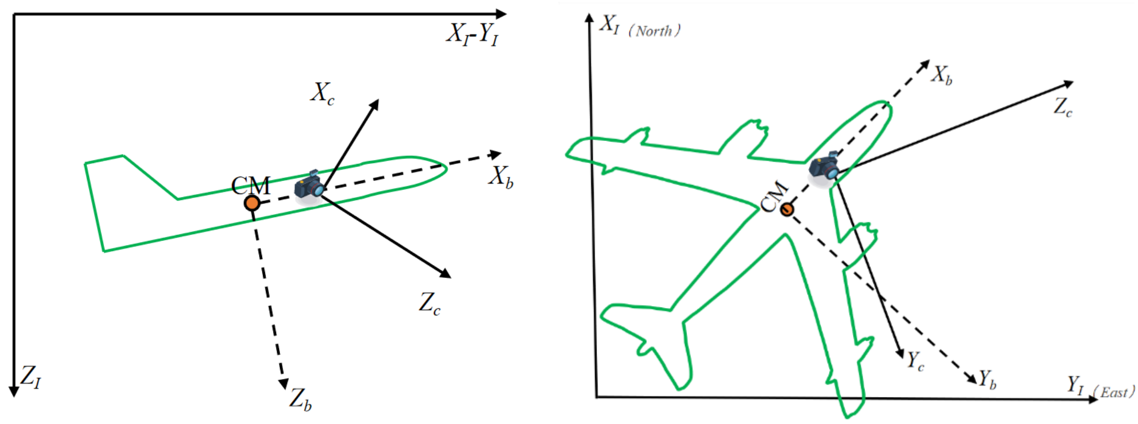

Figure 3. Schematic diagram of the airborne Global Positioning System (GPS) and inertial measurement unit (IMU).

$$\begin{bmatrix} \mathrm{X_A} - \mathrm{X_C} \\ \mathrm{Y_A} - \mathrm{Y_C} \\ \mathrm{Z_A} - \mathrm{Z_C} \end{bmatrix} = \mathrm{C}_b^c \mathrm{C}_e^b \begin{bmatrix} x - x_0 \\ y - y_0 \\ -f \end{bmatrix} \tag{3}$$

Where $\mathrm{X_A}$, $\mathrm{Y_A}$ and $\mathrm{Z_A}$ denote the coordinates of ground points; $\mathrm{X_C}$, $\mathrm{Y_C}$ and $\mathrm{Z_C}$ indicate the origin coordinates of the auxiliary coordinate system; $\mathrm{C_e^b}$ and $\mathrm{C_b^c}$ represent direction cosine matrices from the geodetic coordinate system to the aircraft coordinate system and from the aircraft-body coordinate system to the camera coordinate system.

$\mathrm{C_e^b}$ can be established by the Euler angles between the geodetic coordinate system and the aircraft-body coordinate system. Rotate in the sequence of yaw(ψ), pitch(θ), roll(φ) angles, namely Z-Y-X sequence (Z-Y-X Euler Angles) (4).

$$\mathrm{C}_e^b = \mathrm{C}_X(\varphi) \cdot \mathrm{C}_Y(\theta) \cdot \mathrm{C}_Z(\psi) \tag{4}$$

Where rotating about the Z-axis (ψ).

$$\mathrm{C}_Z(\psi) = \begin{bmatrix} \cos\psi & -\sin\psi & 0 \\ \sin\psi & \cos\psi & 0 \\ 0 & 0 & 1 \end{bmatrix} \tag{5}$$

Rotating about the Y-axis (θ).

$$\mathrm{C}_Y(\theta) = \begin{bmatrix} \cos\theta & 0 & sin\theta \\ 0 & 1 & 0 \\ -sin\theta & 0 & cos\theta \end{bmatrix} \tag{6}$$

Rotating about the X-axis (φ).

$$\mathrm{C}_X(\varphi) = \begin{bmatrix} 1 & 0 & 0 \\ 0 & \cos\varphi & -\sin\varphi \\ 0 & \sin\varphi & \cos\varphi \end{bmatrix} \tag{7}$$

The rotation matrix from the geographic coordinate system to the aircraft-body coordinate system can be expressed as:

$$\mathrm{C}_e^b = \begin{bmatrix} \cos\theta\cos\psi & \cos\theta\sin\psi & -\sin\theta \\ \sin\varphi\sin\theta\cos\psi - \cos\varphi\sin\psi & \sin\varphi\sin\theta\sin\psi + \cos\varphi\cos\psi & \sin\varphi\cos\theta \\ \cos\varphi\sin\theta\cos\psi + \sin\varphi\sin\psi & \cos\varphi\sin\theta\cos\psi - \sin\varphi\sin\psi & \cos\varphi\cos\theta \end{bmatrix} \tag{8}$$

Before the detection of fire points, the GCPs with known coordinates are used to solve the rotation matrix from the aircraft-body coordinate system to the camera coordinate system. It is assumed that there are *i* GCPs with known coordinates, and the equation is constructed as follows:

$$\begin{bmatrix} \mathrm{X_{A1}} & \mathrm{X_{A2}} & \cdots & \mathrm{X_{Ai}} \\ \mathrm{Y_{A1}} & \mathrm{Y_{A2}} & \cdots & \mathrm{Y_{Ai}} \\ \mathrm{Z_{A1}} & \mathrm{Z_{A2}} & \cdots & \mathrm{Z_{Ai}} \end{bmatrix} - \begin{bmatrix} \mathrm{X_C} \\ \mathrm{Y_C} \\ \mathrm{Z_C} \end{bmatrix} = \mathrm{C}_b^c \mathrm{C}_e^b \left(\begin{bmatrix} x_1 & x_2 & \cdots & x_i \\ y_1 & y_2 & \cdots & y_i \\ -f & -f & \cdots & -f \end{bmatrix} - \begin{bmatrix} x_0 \\ y_0 \\ z_0 \end{bmatrix} \right) \tag{9}$$

The above equation is simplified as $\mathrm{A} = \mathrm{C_b^c} \times \mathrm{B}$. Using the optimal estimation method, $\mathrm{C_b^c}$ can be solved by Equation (10).

$$\mathrm{C}_b^c = \left(\mathrm{A^T A}\right)^{-1} \mathrm{A^T B} \tag{10}$$

2.2.3. Estimation of Unknown Target Coordinates

During the fire point positioning and detection using the airborne integrated navigation system, the scale factor of the image needs to be determined, which is calculated by the following formula:

$$\lambda = \frac{Z_S - Z_A}{f} \tag{11}$$

Substituting Equation (11) into Equation (10), Equation (12) can be obtained.

$$\begin{bmatrix} \mathrm{X_A} \\ \mathrm{Y_A} \\ \mathrm{Z_A} \end{bmatrix} = \begin{bmatrix} \mathrm{X_S} \\ \mathrm{Y_S} \\ \mathrm{Z_S} \end{bmatrix} + \lambda \cdot \mathrm{C} \begin{bmatrix} \mathrm{C_{11}} & \mathrm{C_{12}} & \mathrm{C_{13}} \\ \mathrm{C_{21}} & \mathrm{C_{22}} & \mathrm{C_{23}} \\ \mathrm{C_{31}} & \mathrm{C_{32}} & \mathrm{C_{33}} \end{bmatrix} \begin{bmatrix} x - x_0 \\ y - y_0 \\ -f \end{bmatrix} \tag{12}$$

Where C_{ij} ($i = 1, 2, 3; j = 1, 2, 3$) represents the elements of the matrix $\mathrm{C} = \mathrm{C}_b^c \times \mathrm{C}_e^b$.

The GPS adopts the WGS84 coordinate system, and the Earth is a rotating ellipsoid close to a sphere. Thus, points on the ellipsoid can be described by Equation (9).

$$\frac{X_A^2 + Y_A^2}{a^2} + \frac{Z_A^2}{b^2} = 1 \tag{13}$$

Where semi-major axis a = 6,378,137.0 m, and semi-minor axis b = 6,356,752.3142 m.

Solving Equation (12) and Equation (13) together yields Equation (14).

$$\begin{cases} X_A = X_S - \lambda C_{11}(x - x_0) - \lambda C_{12}(y - y_0) + \lambda C_{13} f \\ Y_A = Y_S - \lambda C_{21}(x - x_0) - \lambda C_{22}(y - y_0) + \lambda C_{23} f \\ Z_A = Z_S - \lambda C_{31}(x - x_0) - \lambda C_{32}(y - y_0) + \lambda C_{33} f \end{cases} \tag{14}$$

Actually, the elevation of the fire point location is not zero in general, and a similar elevation H of a fire point can be obtained. Therefore, the fire point is located on an ellipse with the approximate elevation of H, and the fire point location is about to be $Z_A = a + H$.

It is found that the positioning accuracy based on a single image may be influenced by multiple factors such as attitude angle variations, flight altitude and flight stability. In order to improve positioning accuracy, the weighted error correction algorithm is used to achieve accurate fire point positioning by fusing information from multiple images. According to the photogrammetric error theory, the closer to the center of the fire point, the smaller the distortion errors of images. Therefore, flight altitude is fused with phase point coordinates, and it is considered that the higher the flight altitude and the further the phase point is from the center, the larger the detection error.

$$w_i = \frac{1}{H_i^2 + \left(\sqrt{(x - x_0)^2 + (y - y_0)^2}/d\right)^2} \tag{15}$$

Where x_0 and y_0 correspond to the coordinates of principal phase point, x and y denote the coordinates of the corresponding fire point at the phase plane, H_i indicates aircraft flight height of the i-th image, and d indicates the diagonal length of phase amplitude.

Assuming n fire point images are acquired in one detection, with the corresponding coordinates solved as X_i, Y_i, Z_i. The weighting coefficient, w_i, can be derived from Equation (15). Thereby, Equation (16) is established.

$$\begin{cases} X_A = \sum_{i=1}^{n} w_i \lambda_i X_i / \sum_{i=1}^{n} w_i \lambda_i \\ Y_A = \sum_{i=1}^{n} w_i \lambda_i Y_i / \sum_{i=1}^{n} w_i \lambda_i \\ Z_A = \sum_{i=1}^{n} w_i \lambda_i Z_i / \sum_{i=1}^{n} w_i \lambda_i \end{cases} \tag{16}$$

Where X_A, Y_A, Z_A are the weighted coordinates of fire point targets.

3. Results

3.1. Experimental Equipment and Design

In order to verify the effectiveness of the fire positioning model, we select two fire points occurring in the forest region of the Greater Khingan Region within Heilongjiang Province on October 14, 2021. A Y-12 aircraft equipped with high-precision GPS and IMU systems, which can record real-time longitude, latitude, flight altitude, roll, pitch and yaw angles of the aircraft during image acquisition. Detailed configuration parameters of the onboard navigation system are listed in **Table 1**. The airborne camera has 20.1 million effective pixels and an Exmor RS CMOS (Complementary Metal-Oxide-Semiconductor) sensor, ensuring the capture of high-resolution aerial imagery. The camera was mounted on the right-side window of the aircraft, with a fixed focal length of 45 mm to optimize the search field of view and improve image precision.

Table 1. Key parameters of the IMU of the integrated navigation system.

Sensors	Parameters	Value of IMU (GI510)
Gyroscope	Zero bias	0.1 h^{-1}
	Angular random walk	0.03 $h^{-1/2}$
Accelerometer	Zero bias	25 mGal
	Velocity random walk	0.05 $ms^{-1}h^{-1/2}$

During the test, the flight speed was maintained at 230–270 km h^{-1}, and the flight altitude was about 2,000 m to ensure stable image capture under various conditions. In order to reduce the measurement errors caused by rotational discrepancies between the camera and the aircraft body, five fixed locations—intersections of elevated bridges and roads—were selected as the GCPs according to the principles of visibility, distribution, geographical representativeness and stability. These GCPs were precisely measured using high-resolution satellite images, ensuring the uniform distribution of the GCPs across the images and incorporating elevation data of the forest fire detection area. Furthermore, several flight routes were designed according to real-time wildfire conditions to capture fire point images from different angles and evaluate the performance and accuracy of the fire point positioning model (**Figure 4**).

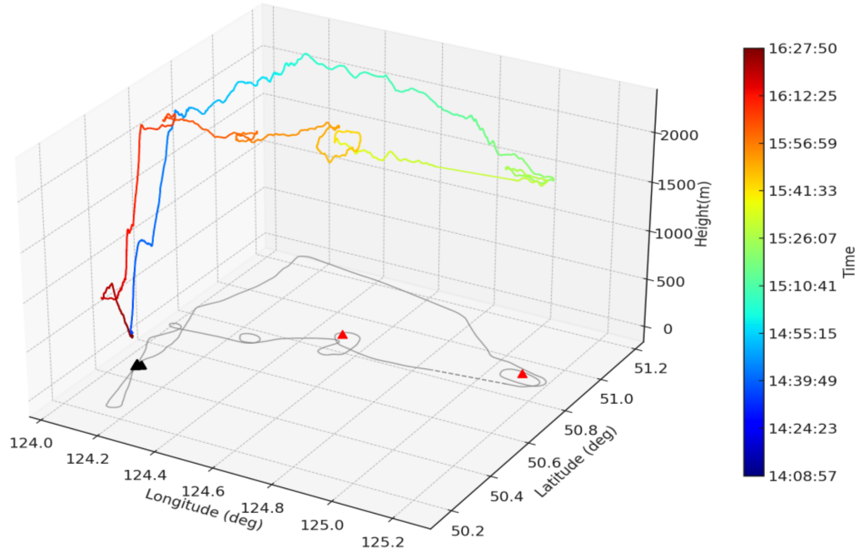

Figure 4. Flight trajectories for fire point detection, ground control points (GCPs) and actual fire point location on October 14, 2021. Red and black triangles represent the actual fire point locations and the GCPs, respectively.

The Greater Khingan Region in Heilongjiang Province is selected as the experimental site. As a high-risk area of forest fires, it provides an ideal environment for testing. The longitudes and latitudes of actual fire points are provided by the Jiagedaqi Aerial Forest Protection Station through on-site surveys, and the authenticity and reliability of fire point locations can be ensured. The experiment conducted in this area is conducive to the effective application of research findings in forest fire monitoring operations and provides a solid foundation for subsequent related research.

3.2. Calibration of Rotation Angles

In order to improve the accuracy of fire point positioning, the rotation angle of the camera relative to the aircraft attitude is calculated based on the longitudes and latitudes of the GCPs and the coordinate transformation algorithm in Section 3.2 (**Figure 5**).

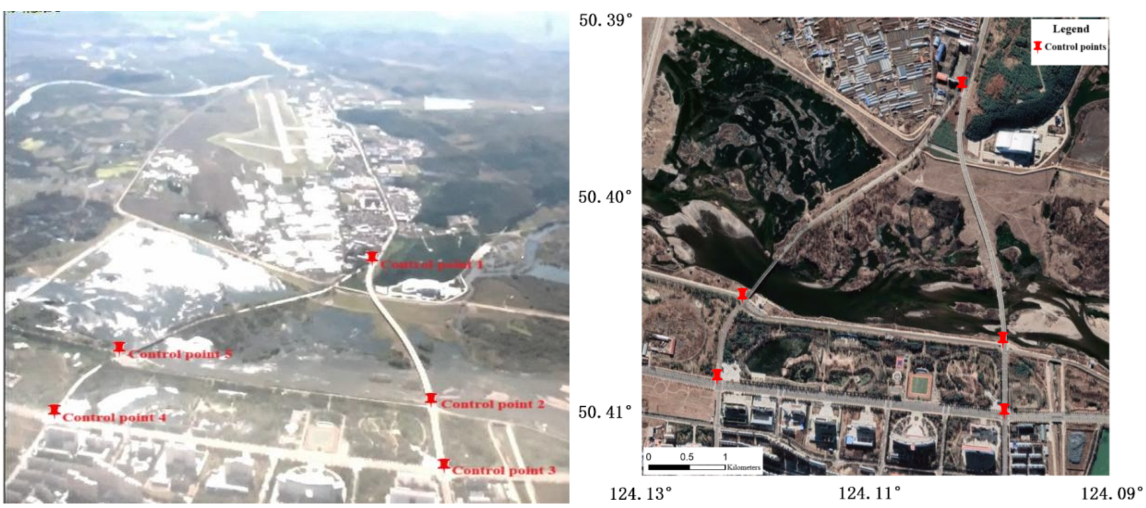

Figure 5. Aerial (left) and satellite (right) images of the GCPs.

The longitudes and latitudes of the GCPs are shown in **Table 2**. The longitude, latitude and flight altitude of the aircraft at the moment of image capture are 124.10843° E, 50.42413° N and 1,970 m, respectively, and the roll, pitching and yaw angles are −0.81°, 0.72° and −60.5°, respectively.

Table 2. Information on the ground control points (GCPs) for camera calibration.

GCPs	Longitude (°)	Latitude (°)	Elevation (m)
1	124.1072722	50.3964194	218.52
2	124.104755	50.40614722	232.15
3	124.1047389	50.4088111	240.51
4	124.1220139	50.40767778	220.12
5	124.1204333	50.40438333	250.21

According to the method proposed in Section 3.2, the coordinate matrix of the five GCPs in the aircraft-body coordinate system A is constructed based on the GCP position information:

$$A = \begin{bmatrix} 711.35 & 1{,}371.11 & -2{,}959.70 \\ 517.53 & 550.16 & -2{,}259.25 \\ 423.08 & 349.17 & -2{,}063.04 \\ -637.87 & 968.86 & -2{,}136.99 \\ -407.51 & 1{,}190.03 & -2{,}350.72 \end{bmatrix}$$

The coordinates of the five GCPs in the phase plane coordinate system are used to establish matrix B:

$$B = \begin{bmatrix} -2{,}219.91 & 1{,}614.45 & -1{,}900.35 \\ -1{,}482.26 & 837.88 & -1{,}666.08 \\ -1{,}312.04 & 616.42 & -1{,}567.13 \\ -2{,}257.48 & 404.36 & -807.91 \\ -2370.38 & 729.80 & -978.21 \end{bmatrix}$$

The matrix C_{bs} is built by using aircraft attitude information, and the rotation matrix from the aircraft-body coordinate system to the phase plane coordinate system is solved. The specific values of the rotation matrix are shown as follows:

$$C_{bs} = \begin{bmatrix} 0.5769 & 0.6472 & -0.4984 \\ -0.4572 & 0.7614 & 0.4596 \\ 0.6769 & -0.0372 & 0.7352 \end{bmatrix}$$

The three rotation angles of the camera relative to the aircraft body, φ, θ and Ψ, are further solved, and their values are −2.9°, −42.6°, and –60.4°, respectively.

To quantitatively validate the localization accuracy of the fire detection model, we planned several flight paths according to the actual conditions of two fire sites to acquire fire imagery from multiple perspectives. Key parameters of flight position and attitude are listed in **Table 3**.

Table 3. Locations and attitude information of the aircraft during the fire point detection.

Fire Points	Number	Longitudes (°)	Latitudes (°)	Altitudes (m)	Flight Speed (km h^{-1})	Heading (°)	Roll Angle φb (°)	Pitching Angle θb (°)	Yaw Angle Ψb (°)
1	Aerial image A	125.10986	50.85944	2,028	235	74	1.21	1.45	26.7
	Aerial image B	125.1298	50.86024	1,992	271	94	0.98	2.16	72.6
2	Aerial image A	124.54142	50.7826	2,034	208	328	2.15	1.86	121.3
	Aerial image B	124.53385	50.79221	2,002	223	337	1.59	0.89	151.4
	Aerial image C	124.53092	50.8157	2,077	221	25	2.16	0.72	210.4
	Aerial image D	124.53835	50.823	2,063	235	39	1.92	2.05	45.3

Based on the several fire point images as shown in **Figures 6** and **7**, the fire point pixel coordinates in the images are converted into the coordinates in the camera coordinate system by the coordinate measurement model for ground targets established in Section 3.1. Applying the rotation angles of the camera relative to the aircraft body obtained in Section 3.2 and the weighted error correction algorithm for multiple images in Subsection 2.2.3, the estimated geolocations of the fire points are calculated (**Table 4**).

Estimation results of the model show that fire points 1 and 2 are located at 125.145984° E, 50.85101° N and 124.54637° E, 50.816106° N, respectively (**Figure 8**). In order to further verify the performance of the model, the estimated locations of the two fire points are compared with the actual fire point locations from the Jiagedaqi Aerial Forest Protection Station. The result indicates that the eastward, northward and horizontal errors are 109.5 m, 112.5 m and 156.99 m for fire point 1, respectively, and are 89.6 m, 123.1 m and 152.21 m for fire point 2, respectively. These results indicate that the proposed positioning model achieves sufficient accuracy for fire detection in forest areas, thus demonstrating the effectiveness of this model.

Aerial image A

Aerial image B

Figure 6. Aerial images for fire point 1.

Aerial image A

Aerial image B

Aerial image C

Aerial image D

Figure 7. Aerial images for fire point 2.

Table 4. Solved fire point information.

Fire Points	Estimated Longitudes (°)	Estimated Latitudes (°)	Observed Longitudes (°)	Observed Latitudes (°)	Eastward Errors (m)	Northward Errors (m)	Horizontal Errors (m)
1	125.145984	50.85101	125.145	50.85	109.5	112.5	156.99
2	124.54637	50.816106	124.545	50.815	89.6	123.1	152.21

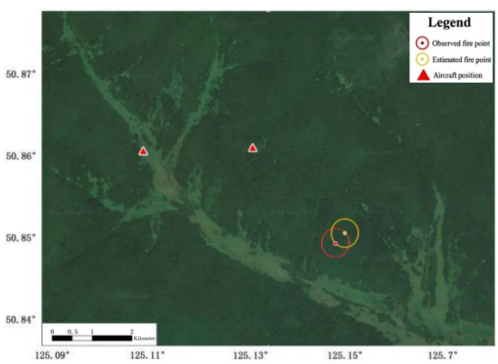

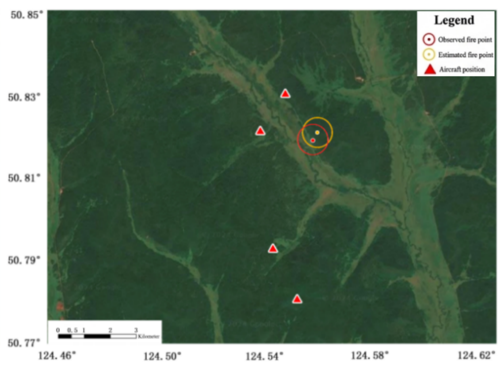

Figure 8. Fire point distribution monitored by satellite remote sensing.

4. Discussion

This study proposes an innovative fire point positioning method based on aerial photography, which integrates multiple technical modules to achieve breakthroughs in positioning accuracy, timeliness, flexibility, and reliability. We discuss the theoretical implications and practical merits of the proposed approach, along with comparisons to existing work, its limitations, and potential avenues for further improvement.

4.1. Theoretical and Practical Implications

On the theoretical side, this work advances the fire point positioning technical system by constructing a multi-module integrated framework that combines ground target coordinate measurement, coordinate system transformation, and cross-image weighted error correction. The accurate conversion method we established between camera and aircraft-body coordinate systems fills a key gap in systematic coordinate alignment for conventional aerial photography positioning, and provides a theoretical foundation for refining aerial positioning techniques in forest fire monitoring.

In practice, our approach resolves several long-standing limitations of traditional fire monitoring systems, including insufficient positioning accuracy, slow data collection, and poor performance under complex fire conditions. Our experimental results show that the horizontal positioning errors for both test fire points are below 160 m, which fully meets the operational requirements of forest fire suppression and allows fire crews to pinpoint fire sources quickly. Compared with satellite-based monitoring, this aerial photography method delivers much better real-time performance, giving decision-makers timely access to up-to-date fire dynamics. This enables flexible adjustments to firefighting strategies and improves overall emergency response efficiency. Additionally, the high flexibility of aerial imaging supports multi-angle and scenario-adaptive monitoring, making it particularly valuable for analyzing fire spread patterns and assessing burned areas in complex terrain such as mountainous forests.

4.2. Comparison with Previous Research

Current fire point positioning methods are largely dependent on satellite remote sensing and ground-based monitoring. While satellite remote sensing offers broad coverage over large areas, it suffers from low spatial resolution and long data return intervals, leading to weak real-time performance and trouble in precisely locating small-scale fire incidents. Ground-based monitoring (e.g., surveillance cameras, fire watchtowers) has high local positioning accuracy but is restricted by geographical conditions and has a narrow monitoring range.

The method proposed in this study complements and optimizes the existing technical system. Compared with satellite-based methods, it significantly improves real-time performance and positioning accuracy for small to medium-sized fires; compared with ground-based methods, it expands the monitoring range and enhances adaptability to complex terrains. Previous studies on aerial photography-based fire positioning have rarely integrated multi-image weighted error correction algorithms, leading to significant errors caused by camera attitude changes. This study introduces this algorithm to effectively reduce such errors, improving the reliability and stability of positioning, which is a key advantage over similar aerial-based studies.

Compared with the SfM, the proposed method directly obtains high-precision flight parameters through GPS/IMU equipment and embeds a multi-image weighted error correction algorithm into the overall workflow. This technical design reduces the reliance on original image quality and lowers relevant environmental interference sensitivity, rendering the method highly applicable to dynamic wildfire scenarios with complex and variable conditions such as smoke occlusion.

Compared with the DG, the approach developed in this study adopts a multi-image correction framework integrated with a dynamic error weighting strategy, which substantially suppresses positioning drift in complex terrain environments. Experimental verification demonstrates that the comprehensive positioning error can be stabilized within 160 m. In contrast, the conventional DG method is primarily applicable to fixed-wing platforms and high-altitude unmanned aerial vehicles operating above 3,000 m, affording superior overall operational safety.

4.3. Research Limitations

While the method proposed in this paper performs well in real applications, it still has certain inherent limitations. First, the experimental validation was only conducted under limited airborne observation scenarios, and the adaptability of the proposed method under extreme weather [40] (e.g., dense fog, torrential rain and strong gales) remains insufficiently evaluated. Harsh meteorological conditions can degrade aerial image quality and reduce the precision of coordinate transformation [41]. To overcome the above deficiency, we will integrate multispectral and infrared fusion strategies to achieve more stable fire monitoring amid extreme meteorological conditions. Second, the current method focuses on fire point positioning and has not yet realized the quantitative evaluation of key fire parameters such as burned area and fire intensity [42]. Although it has the potential for such evaluation, additional algorithm optimization and data calibration are needed [43,44]. Particular emphasis will be given to enhancing positioning accuracy in complex terrain and realizing the inversion of key fire parameters. Third, the method relies on aerial platforms (e.g., Unmanned Aerial Vehicles—UAVs, helicopters), and the operational range and duration are limited by the platform's battery life and load capacity [45–47], which may restrict its application in large-scale, long-duration forest fire monitoring [48,49]. Further optimization of the IMU/GPS filtering algorithm will also be considered to promote attitude measurement accuracy amid drastic motion of the airborne platform.

4.4. Future Research Directions

To address the above limitations and further improve the method's application value, future research can focus on the following directions: (1) Conduct experiments under extreme weather conditions to optimize the algorithm's anti-interference ability, such as introducing image enhancement technologies to improve the quality of aerial images in low-visibility environments. (2) Expand the application scope of the method by developing quantitative evaluation models for burned area, fire intensity, and other parameters based on multi-angle aerial images, realizing comprehensive fire situation assessment. (3) Explore the integration of aerial photography-based positioning with satellite remote sensing data. By combining the large-scale coverage advantage of satellites and the high-precision, real-time advantages of aerial photography, a multi-level, comprehensive forest fire monitoring system can be established. (4) Future research can explore the development of low-cost, long-endurance aerial platforms and intelligent flight control systems, which will effectively improve the operational efficiency and monitoring coverage of this method in large-scale forest fire monitoring.

5. Conclusions

In this study, we've developed a new fire point positioning method based on aerial photography, which integrates the ground target coordinate measurement model, precise coordinate system conversion, and a multi-image weighted error correction algorithm. We ran actual airborne tests to validate its performance and identify its advantages over existing methods—and after confirming its effectiveness, we've drawn the following main conclusions:

1. It delivers highly accurate fire point localization. For the two test fire points, horizontal positioning errors were measured at 156.99 m and 152.21 m, both well below the 160-m threshold. By combining the ground target coordinate measurement model with rigorous coordinate system transformation, we effectively suppressed measurement deviations, laying a solid foundation for precise fire-suppression operations.
2. Our approach uses a multi-image weighted error correction algorithm that improves overall positioning accuracy while boosting the reliability and stability of the entire scheme. In practical use, it significantly reduces interference from camera attitude angle variations and performs particularly well in multi-source image fusion processing.
3. Compared with conventional satellite monitoring methods, this technique offers far better real-time performance. It allows for fast fire data acquisition and transmission, enabling timely adjustments to firefighting strategies and improving overall emergency response efficiency.
4. It also provides considerable operational flexibility, as we can adapt monitoring strategies and flight routes in real time in response to changing fire behavior. It supports multi-angle image capture of fire events and has clear practical value in assessing fire location, burned area, fire line length, and fire propagation trends.

Overall, the fire point positioning method developed in this study offers a practical and effective technical solution for real-world forest fire monitoring and emergency response.

It helps improve the accuracy of fire point localization, minimize wildfire losses, and provide a sound foundation for scientific decision-making in forest fire prevention and management. Going forward, we will focus on combining this approach with satellite remote sensing data and improving its quantitative assessment capabilities, which will further enhance the comprehensiveness and efficiency of forest fire monitoring systems and offer more reliable support for the sustainable management of forest ecosystems.

Author Contributions

Conceptualization, Y.A.; methodology, S.H.; validation, Y.J.; investigation, X.S.; data curation, S.W.; writing—original draft preparation, Y.A. and S.H.; writing—review and editing, Y.A. and S.H.; project administration, Y.A. All authors have read and agreed to the published version of the manuscript.

Funding

This work was funded by the Innovation and Development Special Project of China Meteorological Administration (project No. CXFZ2024J028).

Institutional Review Board Statement

Not applicable.

Informed Consent Statement

Not applicable.

Data Availability Statement

This study did not generate any new data. All data analyzed during the research are publicly available from official repositories, and the relevant sources have been clearly cited in the manuscript.

Conflicts of Interest

The authors declare no conflict of interest.

AI Use Statement

During the preparation of this manuscript, the authors used DeepSeek solely for language refinement. No AI tools were used for data analysis, interpretation, or generation of scientific content. All outputs were critically reviewed and edited by the authors. The authors take full responsibility for the integrity and accuracy of the work.

References

[1] Certini, G., 2005. Effects of Fire on Properties of Forest Soils: A Review. Oecologia. 143(1), 1–10.

[2] Bowman, D.M.J.S., Balch, J.K., Artaxo, P., et al., 2009. Fire in the Earth system. Science. 324(5926), 481–484.

[3] Arana, P.V., Cabrera, A.F., Perez, M.J., et al., 2018. Challenges of an autonomous wildfire geolocation system based on synthetic vision technology. Sensors. 18(11), 3631.

[4] Zhang, Z., Zhang, T., Zeng, W., et al., 2025. Application Progress of Forest Fire Monitoring Based on Satellite Remote Sensing. Journal of Southwest Forestry University. 45(6), 211–220. (in Chinese)

[5] Roberts, G., Wooster, M.J., 2014. Development of a multi-temporal Kalman filter approach to geostationary active fire detection & fire radiative power (FRP) estimation. Remote Sensing of Environment. 152, 392–412.

[6] Liu, X., He, B., Quan, X., et al., 2018. Near real-time extracting wildfire spread rate from Himawari-8 satellite data. Remote Sensing. 10(10), 1654.

[7] Moreno, M.V., Laurent, P., Ciais, P., et al., 2020. Assessing satellite-derived fire patches with functional diversity trait methods. Remote Sensing of Environment. 247, 111897.

[8] Zheng, W., Chen, J., Tang, S.H., et al., 2020. Fire monitoring based on FY-3D/MERSI-II far-infrared data. Journal of Infrared and Millimeter Waves. 39(1), 120–127. (in Chinese)

[9] Roberts, G., Wooster, M.J., Perry, G.L.W., et al., 2005. Retrieval of biomass combustion rates and totals from fire radiative power observations: Application to southern Africa using geostationary SEVIRI imagery. Journal of Geophysical Research: Atmospheres. 110, D21111.

[10] Rao, Y., Wang, C., Huang, H., 2020. Forest fire monitoring based on multisensor remote sensing techniques in Muli County, Sichuan Province. Journal of Remote Sensing. 24(5), 559–570. (in Chinese)

[11] Chung, Y.S., Kim, H.S., 2008. Satellite monitoring of forest fires and associated smoke plumes occurring in Korea. Air Quality, Atmosphere & Health. 1(2), 111–118.

[12] Jones, H.G., Sirault, X.R.R., 2014. Scaling of Thermal Images at Different Spatial Resolution: The Mixed Pixel Problem. Agronomy. 4(3), 380–396.

[13] Güney, O.C., Mert, A., Gülsoy, S., 2023. Assessing fire severity in Turkey's forest ecosystems using spectral indices from satellite images. Journal of Forestry Research. 34(6), 1747–1761.

[14] Lin, Z., Chen, F., Niu, Z., et al., 2018. An active fire detection algorithm based on multi-temporal FengYun-3C VIRR data. Remote Sensing of Environment. 211, 376–387.

[15] Chen, Y., Morton, D.C., Randerson, J.T., 2024. Remote sensing for wildfire monitoring: Insights into burned area, emissions, and fire dynamics. One Earth. 7(6), 1022–1028.

[16] Zhao, Y., Ma, J., Li, X., et al., 2018. Saliency Detection and Deep Learning-Based Wildfire Identification in UAV Imagery. Sensors. 18(3), 712.

[17] Bouguettaya, A., Zarzour, H., Taberkit, A.M., et al., 2022. A Review on Early Wildfire Detection from Unmanned Aerial Vehicles using Deep Learning-Based Computer Vision Algorithms. Signal Processing. 190, 108309.

[18] Titu, M.F.S., Pavel, M.A., Michael, G.K.O., et al., 2024. Real-Time Fire Detection: Integrating Lightweight Deep Learning Models on Drones with Edge Computing. Drones. 8(9), 483.

[19] Shamsoshoara, A., Afghah, F., Razi, A., et al., 2021. Aerial imagery pile burn detection using deep learning: The FLAME dataset. Computer Networks. 193, 108001.

[20] Xu, Y., Li, J., Zhang, F., 2022. A UAV-Based Forest Fire Patrol Path Planning Strategy. Forests. 13(11), 1952.

[21] Wijikumar, P., Partheepan, S., Hassan, J., et al., 2025. Transfer Learning-Enhanced Gradient Boosting Models for Wildfire Detection Using UAV Imagery. In Proceedings of the 26th IEEE International Symposium on a World of Wireless, Mobile and Multimedia Networks (WoWMoM), Fort Worth, TX, USA, 27–30 May 2025; pp. 311–316.

[22] Viseras, A., Marchal, J., Schaab, M., et al., 2019. Wildfire monitoring and hotspots detection with aerial robots: Measurement campaign and first results. In Proceedings of the IEEE International Symposium on Safety, Security, and Rescue Robotics (SSRR), Würzburg, Germany, 2–4 September 2019; pp. 102–103.

[23] Marčiš, M., Fraštia, M., Lieskovský, T., et al., 2024. Photogrammetric Measurement of Grassland Fire Spread: Techniques and Challenges with Low-Cost Unmanned Aerial Vehicles. Drones. 8(7), 282.

[24] Wei, Y., Kang, L., Yang, B., et al., 2013. Applications of structure from motion: A survey. Journal of Zhejiang University-Science C (Computers & Electronics). 14(7), 486–494.

[25] Iglhaut, J., Cabo, C., Puliti, S., et al., 2019. Structure from Motion Photogrammetry in Forestry: A Review. Current Forestry Reports. 5(3), 155–168.

[26] Fernández, G.J.M., Calvo, L., Pérez, R.L.A., et al., 2024. Integrating Physical-Based Models and Structure-from-Motion Photogrammetry to Retrieve Fire Severity by Ecosystem Strata from Very High Resolution UAV Imagery. Fire. 7(9), 304.

[27] Özyeşil, O., Voroninski, V., Basri, R., et al., 2017. A survey of structure from motion. Acta Numerica. 26, 305–364.

[28] Cao, M., Cao, L., Jia, W., et al., 2018. Evaluation of local features for structure from motion. Multimedia Tools and Applications. 77(9), 10979–10993.

[29] Umar, M.M., De Silva, L.C., 2017. Fire boundary detection method using a unique structure from motion for non-rigid bodies algorithm (SFM-NRBA). In Proceedings of the 9th International Conference on Signal Processing Systems, Auckland, New Zealand, 27–30 Novemnber 2017; pp. 74–78.

[30] Mlambo, R., Woodhouse, I.H., Gerard, F., et al., 2017. Structure from motion (SfM) photogrammetry with drone data: A low cost method for monitoring greenhouse gas emissions from forests in developing countries. Forests. 8(3), 68.

[31] Losso, A., Corgnati, L., Perona, G., 2010. Innovative image geo-referencing tool for decision support in wildfire fighting. WIT Transactions on Ecology and the Environment. 137, 173–183.

[32] Sargento, F., Ribeiro, R., Cherif, E.K., et al., 2022. Real-Time Georeferencing of Fire Front Aerial Images Using Structure from Motion and Iterative Closest Point. In: Rousseau, J.J., Kapralos, B. (Eds.). Pattern Recognition, Computer Vision, and Image Processing. ICPR 2022 International Workshops and Challenges (ICPR 2022), Vol. 13644: Lecture Notes in Computer Science. Springer: Cham, Switzerland. 194–202.

[33] El-Sheimy, N., Wright, B., 2005. The development and testing of a prototype mobile mapping system for real-time forest fire hot spot detection. Photogrammetric Engineering & Remote Sensing. 71(4), 461–470.

[34] Santana, B., Cherif, E.K., Bernardino, A., et al., 2022. Real-Time Georeferencing of Fire Front Aerial Images Using Iterative Ray-Tracing and the Bearings-Range Extended Kalman Filter. Sensors. 22(3), 1150.

[35] Guo, C., Lu, F., Deng, Z., et al., 2023. Fast and Reliable Convergence of Real-Time Kinematic Single Point Positioning Using Equivalent Elimination Principle. Geomatics and Information Science of Wuhan University. 48(7), 1117–1125. (in Chinese)

[36] Chen, X., Hopkins, B., Wang, H., et al., 2022. Wildland fire detection and monitoring using a drone-collected RGB/IR image dataset. In Proceedings of the 2022 IEEE Applied Imagery Pattern Recognition Workshop (AIPR), Washington, DC, USA, 11–13 October 2022;

pp. 1–4.
[37] Partheepan, S., Sanati, F., Hassan, J., 2023. Autonomous Unmanned Aerial Vehicles in Bushfire Management: Challenges and Opportunities. Drones. 7(47), 47.
[38] Chuvieco, E., Aguado, I., Salas, J., et al., 2020. Satellite remote sensing contributions to wildland fire science and management. Current Forestry Reports. 6(2), 81–96.
[39] Zhang, Z., 1999. Flexible camera calibration by viewing a plane from unknown orientations. In Proceedings of the Seventh IEEE International Conference on Computer Vision, Kerkyra, Greece, 20–27 September 1999; pp. 666–673.
[40] Wang, D., Jia, Z., Xia, Y., et al., 2021. Research Progress and Trend in Forestry and Grassland Fires Monitoring Technology. World Forestry Research. 34(2), 26–32. (in Chinese)
[41] Yogender, Raghavendra, S., Kushwaha, S.K.P., 2020. Role of Ground Control Points (GCPs) in Integration of Terrestrial Laser Scanner (TLS) and Close-range Photogrammetry (CRP). In: Ghosh, J.K., da Silva, I. (Eds.). Applications of Geomatics in Civil Engineering: Select Proceedings of ICGCE 2018, Vol. 33: Lecture Notes in Civil Engineering. Springer: Singapore. pp. 531–537.
[42] He, Y., Yang, J., Ma, Y., et al., 2016. A method for fire detection using Landsat 8 data. Journal of Infrared and Millimeter Waves. 35(5), 600–608, 624. (in Chinese)
[43] Freeborn, P.H., Wooster, M.J., Roy, D.P., et al., 2014. Quantification of MODIS fire radiative power (FRP) measurement uncertainty for use in satellite-based active fire characterization and biomass burning estimation. Geophysical Research Letters. 41(6), 1988–1994.
[44] Fu, Y., Li, R., Wang, X., et al., 2020. Fire Detection and Fire Radiative Power in Forests and Low-Biomass Lands in Northeast Asia: MODIS versus VIIRS Fire Products. Remote Sensing. 12(18), 2870.
[45] Giitsidis, T., Karakasis, E.G., Gasteratos, A., et al., 2015. Human and Fire Detection from High Altitude UAV Images. 2015 23rd Euromicro International Conference on Parallel, Distributed, and Network-Based Processing, Turku, Finland, 4–6 March 2015; pp. 309–315.
[46] Alexis, K., Nikolakopoulos, G., Tzes, A., et al., 2009. Coordination of Helicopter UAVs for Aerial Forest-Fire Surveillance. In: Valavanis, K.P. (Ed.). Applications of Intelligent Control to Engineering Systems. Intelligent Systems, Control, and Automation: Science and Engineering, Vol. 39. Springer: Dordrecht, The Netherlands. pp. 169–193.
[47] Luan, T., Zhou, S., Zhang, G., et al., 2024. Enhanced Lightweight YOLOX for Small Object Wildfire Detection in UAV Imagery. Sensors. 24(9), 2710.
[48] Kumar, M., Cohen, K., 2009. Wild Land Fire Fighting Using Multiple Uninhabited Aerial Vehicles. In Proceedings of the AIAA Infotech @ Aerospace Conference, Seattle, WA, USA, 6–9 April 2009.
[49] Abdusalomov, A., Umirzakova, S., Bakhtiyor, S.M., et al., 2024. Drone-Based Wildfire Detection with Multi-Sensor Integration. Remote Sensing. 16(24), 4651.